

Supporting Information

In situ Formation of Tungsten Oxycarbide, Tungsten Carbide and Tungsten Nitride Nanoparticles in Micro- and Mesoporous Polymer-Derived Ceramics

Mahdi Seifollahi Bazarjani,^{1,2*} Mathis M. Müller,¹ Hans-Joachim Kleebe,¹ Claudia Fasel,¹ Ralf Riedel¹, and Aleksander Gurlo¹

¹ – *Technische Universität Darmstadt, Fachbereich Material-und Geowissenschaften, Jovanka Bontschits Str. 2, D-64287 Darmstadt, Germany*

² – *Carl von Ossietzky Universität Oldenburg, Institute für Chemie, Carl von Ossietzky Str. 9-11, D-26129 Oldenburg, Germany*

* mahdi.seifollahi.bazarjani@uni-oldenburg.de

Thermolysis profiles

- 1) 200 °C: from room temperature (r.t.) to 200 °C with the rate of 50 °C h⁻¹, holding at 200 °C for 2 h, cooling to r.t. with the rate of 50 °C h⁻¹;
- 2) 300 °C: from r.t. to 200 °C with the rate of 50 °C h⁻¹, holding at 200 °C for 2 h, from 200 °C to 300 °C with the rate of 50 °C h⁻¹, holding at 300 °C for 2 h and cooling to r.t. with the rate of 50 °C h⁻¹;
- 3) 500 °C: from r.t. to 200 °C with the rate of 50 °C h⁻¹, holding at 200 °C for 2 h, from 200 °C to 500 °C with the rate of 50 °C h⁻¹, holding at 500 °C for 2 h and cooling to r.t. with the rate of 50 °C h⁻¹;
- 4) 700 °C: from r.t. to 200 °C with the rate of 50 °C h⁻¹, holding at 200 °C for 2 h, from 200 °C to 600 °C with the rate of 50 °C h⁻¹, holding at 600 °C for 2 h, from 600 °C to 700 °C with the rate of 25 °C h⁻¹, holding at 700 °C for 1 h, and cooling to r.t. with the rate of 50 °C h⁻¹;
- 5) 800 °C: from r.t. to 200 °C with the rate of 50 °C h⁻¹, holding at 200 °C for 2 h, from 200 °C to 600 °C with the rate of 50 °C h⁻¹, holding at 600 °C for 2 h, from 600 °C to 800 °C with the rate of 25 °C h⁻¹, holding at 800 °C for 1 h, and cooling to r.t. with the rate of 50 °C h⁻¹;
- 6) 900 °C: from r.t. to 200 °C with the rate of 50 °C h⁻¹, holding at 200 °C for 2 h, from 200 °C to 600 °C with the rate of 50 °C h⁻¹, holding at 600 °C for 2 h, from 600 °C to 900 °C with the rate of 25 °C h⁻¹, holding at 900 °C for 1 h, and cooling to r.t. with the rate of 50 °C h⁻¹;
- 7) 1000 °C: from r.t. to 200 °C with the rate of 50 °C h⁻¹, holding at 200 °C for 2 h, from 200 °C to 600 °C with the rate of 50 °C h⁻¹, holding at 600 °C for 2 h, from 600 °C to 1000 °C with the rate of 25 °C h⁻¹, holding at 1000 °C for 1 h, and cooling to r.t. with the rate of 50 °C h⁻¹;

8) 1100 °C: from r.t. to 200 °C with the rate of 50 °C h⁻¹, holding at 200 °C for 2 h, from 200 °C to 600 °C with the rate of 50 °C h⁻¹, holding at 600 °C for 2 h, from 600 °C to 1100 °C with the rate of 25 °C h⁻¹, holding at 1100 °C for 1 h, and cooling to r.t. with the rate of 50 °C h⁻¹;

9) 1200 °C: from r.t. to 200 °C with the rate of 50 °C h⁻¹, holding at 200 °C for 2 h, from 200 °C to 600 °C with the rate of 50 °C h⁻¹, holding at 600 °C for 2 h, from 600 °C to 1200 °C with the rate of 25 °C h⁻¹, holding at 1200 °C for 1 h, and cooling to r.t. with the rate of 50 °C h⁻¹;

10) 1300 °C: from r.t. to 200 °C with the rate of 50 °C h⁻¹, holding at 200 °C for 2 h, from 200 °C to 600 °C with the rate of 50 °C h⁻¹, holding at 600 °C for 2 h, from 600 °C to 1300 °C with the rate of 25 °C h⁻¹, holding at 1300 °C for 1 h, and cooling to r.t. with the rate of 50 °C h⁻¹;

XRD patterns of thermolysis products at 1300 °C, leading to the formation of Silicon oxycarbide (SiOC, indicated with blue color in Figure S1) ceramic using [-Si(O)CH₂-]_n as initial precursor and WC/SiOC naniocomposites using 10/c-WO_{3-x}/WO₃×H₂O/[-Si(O)CH₂-]_n, 20/c-WO_{3-x}/WO₃×H₂O/[-Si(O)CH₂-]_n and 30/c-WO_{3-x}/WO₃×H₂O/[-Si(O)CH₂-]_n as initial precursors

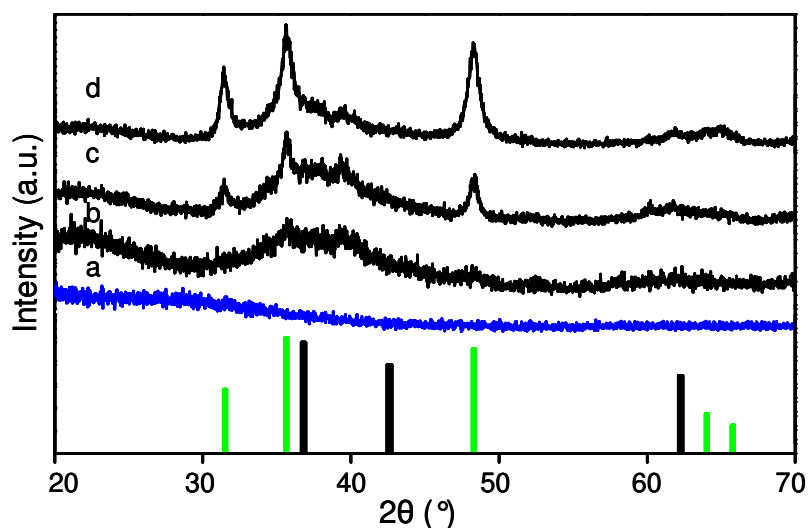


Figure S1. XRD patterns of specimens produced by thermolysis at 1300 °C of [-Si(O)CH₂-]_n (a), 10/c-WO_{3-x}/WO₃×H₂O/[-Si(O)CH₂-]_n (b), 20/c-WO_{3-x}/WO₃×H₂O/[-Si(O)CH₂-]_n (c) and 30/c-WO₃₋

x /WO₃ \times H₂O/[Si(O)CH₂-]_n (d). The black columns refer to pattern of tungsten oxycarbide (W₂CO, PDF Nr.: 22-0959, space group *Fm-3m*, No 225, Z=2, a=4.2400 Å), the green columns refer to pattern of tungsten carbide (WC, PDF Nr.: 89-2727, space group *P-6m2*, No 187, Z=1, a=2.9060 Å, c=2.8370 Å).

SEM micrographs of [-Si(O)CH₂-]_n, 10/c-WO_{3-x}/WO₃ \times H₂O/[Si(O)CH₂-]_n, 20/c-WO_{3-x}/WO₃ \times H₂O/[Si(O)CH₂-]_n and 30/c-WO_{3-x}/WO₃ \times H₂O/[Si(O)CH₂-]_n

The secondary electron microscopy micrographs of the specimens produced after thermolysis at 700, 900, 1100 and 1300 °C of the 10/c-WO_{3-x}/WO₃ \times H₂O/[Si(O)CH₂-]_n, 20/c-WO_{3-x}/WO₃ \times H₂O/[Si(O)CH₂-]_n and 30/c-WO_{3-x}/WO₃ \times H₂O/[Si(O)CH₂-]_n nanocomposites are shown in Figure S2. The morphologies of the samples produced at 700, 900 and 1100 °C are similar to the initial nanocomposites before thermolysis (compare Figure S2 and Figure S3). On the other hand, the samples thermolyzed at 1300 °C reveal significant formation of whiskers and the amount of whiskers increases as the tungsten content increases (Figure S4(a, b), (c, d), and (e, f)).

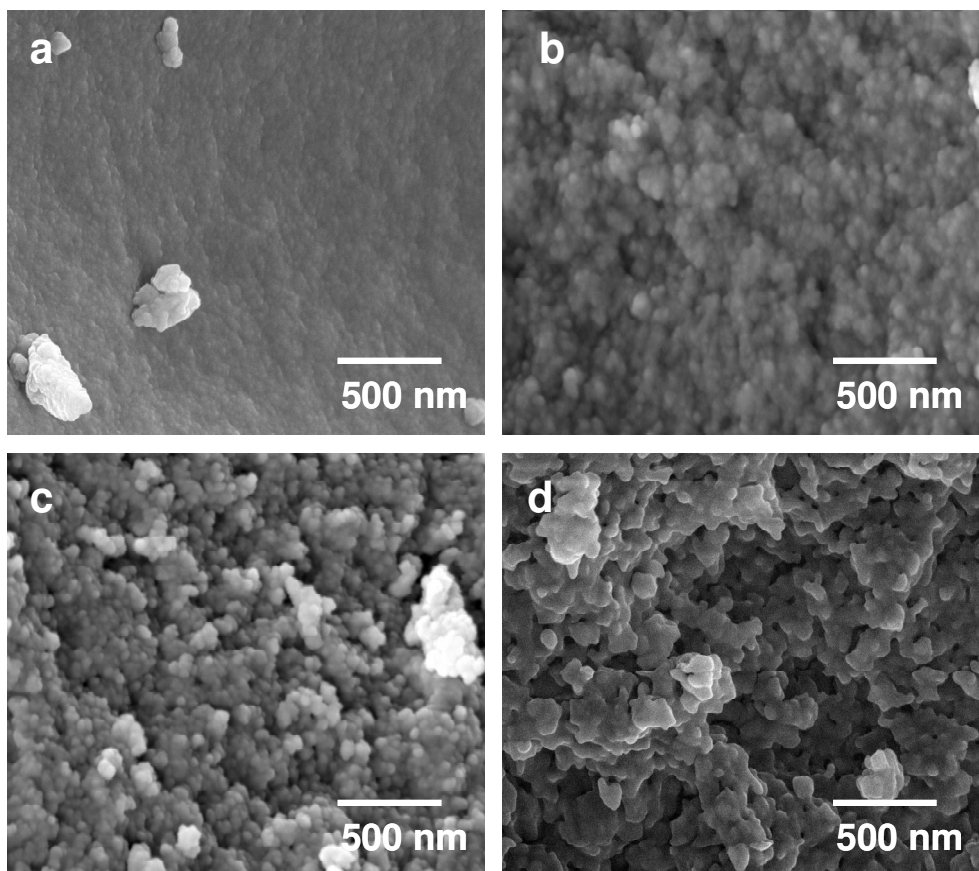


Figure S2. SEM images of the $[-\text{Si}(\text{O})\text{CH}_2-]_n$ (a), $10/\text{C-WO}_{3-x}/\text{WO}_3 \times \text{H}_2\text{O}/[-\text{Si}(\text{O})\text{CH}_2-]_n$ (b), $20/\text{C-WO}_{3-x}/\text{WO}_3 \times \text{H}_2\text{O}/[-\text{Si}(\text{O})\text{CH}_2-]_n$ (c) and $30/\text{C-WO}_{3-x}/\text{WO}_3 \times \text{H}_2\text{O}/[-\text{Si}(\text{O})\text{CH}_2-]_n$ (d) with 0, 10, 20 and 30 wt % of c- $\text{WO}_{3-x}/\text{WO}_3 \times \text{H}_2\text{O}$ nanowiskers, respectively. The samples are coated with a thin layer of gold to provide conductivity.

SEM micrographs of $[-\text{Si}(\text{O})\text{CH}_2-]_n$, $10/\text{c-WO}_{3-x}/\text{WO}_3 \times \text{H}_2\text{O}/[-\text{Si}(\text{O})\text{CH}_2-]_n$, $20/\text{c-WO}_{3-x}/\text{WO}_3 \times \text{H}_2\text{O}/[-\text{Si}(\text{O})\text{CH}_2-]_n$ and $30/\text{c-WO}_{3-x}/\text{WO}_3 \times \text{H}_2\text{O}/[-\text{Si}(\text{O})\text{CH}_2-]_n$ after thermolysis at 700, 900, 1100 and 1300 °C

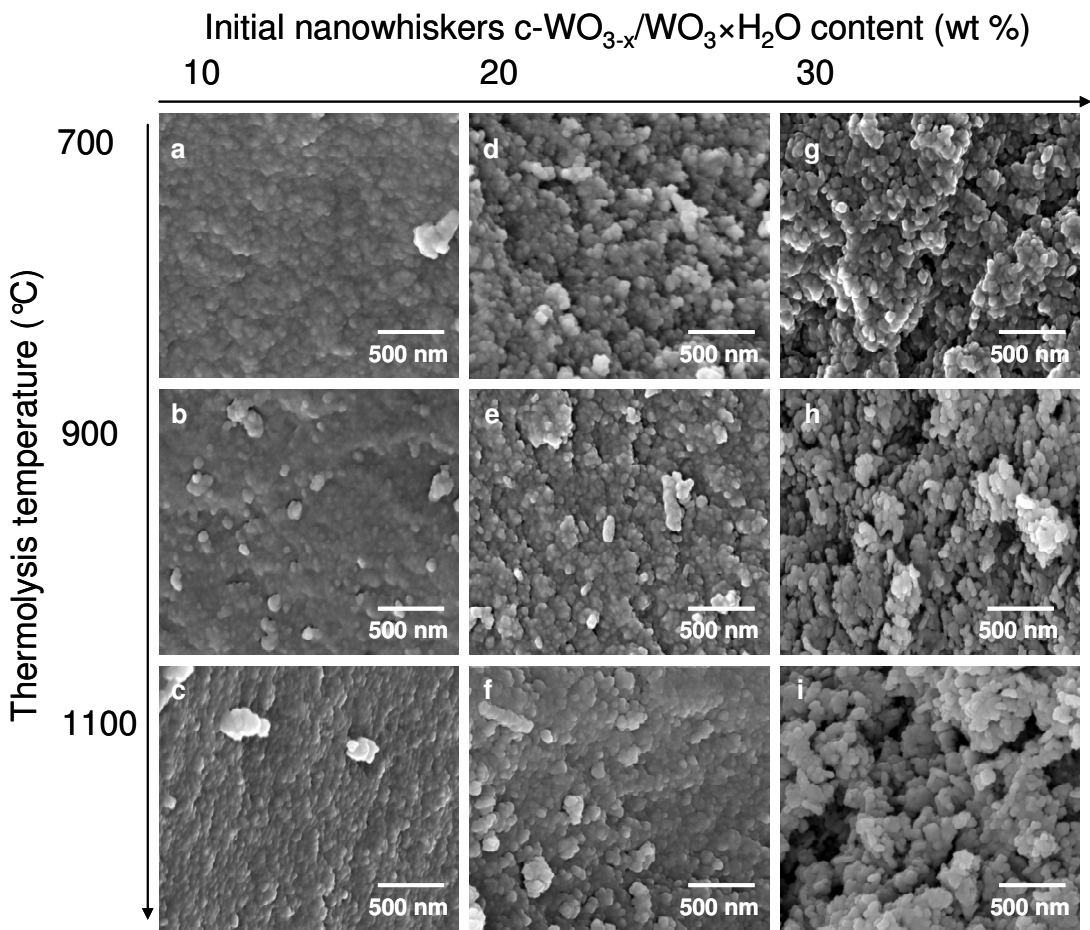


Figure S3. SEM images of the thermolysis products at 700 °C (a, d, and g), 900 °C (b, e and h) and 1100 °C (c, f, i) of $10/\text{c-WO}_{3-x}/\text{WO}_3 \times \text{H}_2\text{O}/[-\text{Si}(\text{O})\text{CH}_2-]_n$ (a, b and c), $20/\text{c-WO}_{3-x}/\text{WO}_3 \times \text{H}_2\text{O}/[-\text{Si}(\text{O})\text{CH}_2-]_n$ (d, e and f), and $30/\text{c-WO}_{3-x}/\text{WO}_3 \times \text{H}_2\text{O}/[-\text{Si}(\text{O})\text{CH}_2-]_n$ (g, h and i). The samples are coated with a thin layer of gold to provide conductivity.

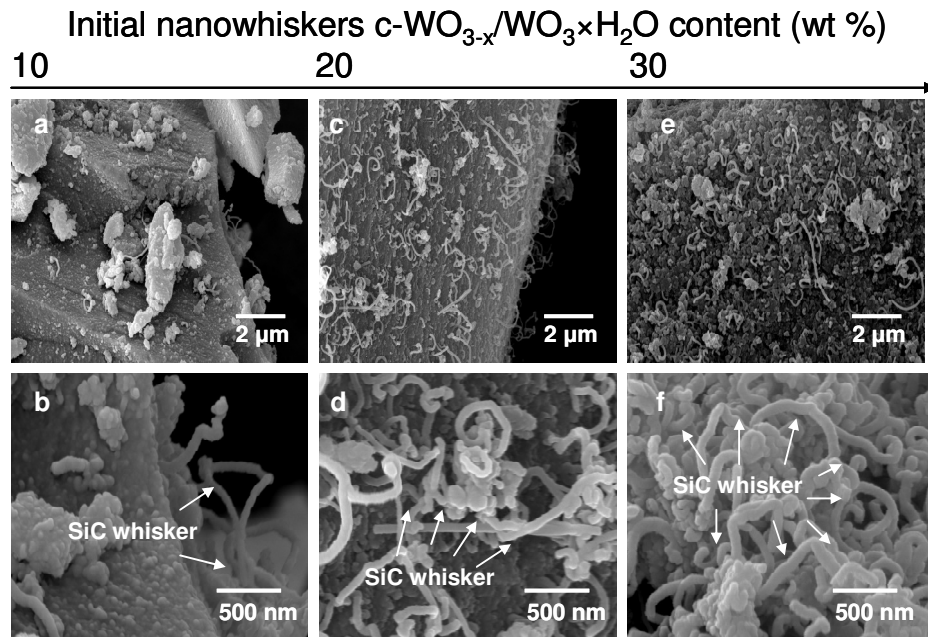


Figure S4. SEM images of the thermolysis products at 1300 °C of 10/c-WO_{3-x}/WO₃×H₂O/[$\text{-Si(O)CH}_2\text{-}]_n$ (a, b), 20/c-WO_{3-x}/WO₃×H₂O/[$\text{-Si(O)CH}_2\text{-}]_n$ (c, d) and 30/c-WO_{3-x}/WO₃×H₂O/[$\text{-Si(O)CH}_2\text{-}]_n$ (e, f). The samples are coated with a thin layer of gold to provide conductivity. SiC whiskers are indicated with white arrows.

Thermal gravimetric analysis of [$\text{-Si(O)CH}_2\text{-}]_n$, 10/c-WO_{3-x}/WO₃×H₂O/[$\text{-Si(O)CH}_2\text{-}]_n$, 20/c-WO_{3-x}/WO₃×H₂O/[$\text{-Si(O)CH}_2\text{-}]_n$ and 30/c-WO_{3-x}/WO₃×H₂O/[$\text{-Si(O)CH}_2\text{-}]_n$

Thermal gravimetric analysis is performed under Ar atmosphere (Figure S5). [$\text{-Si(O)CH}_2\text{-}]_n$ hybrid polymer shows a stable ceramic yield of ~ 80 % at 900 °C. The initial mass losses in the 20/c-WO_{3-x}/WO₃×H₂O/[$\text{-Si(O)CH}_2\text{-}]_n$ and 30/c-WO_{3-x}/WO₃×H₂O/[$\text{-Si(O)CH}_2\text{-}]_n$ nanocomposites are less than the native [$\text{-Si(O)CH}_2\text{-}]_n$. However, at above 1000 °C significant mass losses in the 30/c-WO_{3-x}/WO₃×H₂O/[$\text{-Si(O)CH}_2\text{-}]_n$ and 20/c-WO_{3-x}/WO₃×H₂O/[$\text{-Si(O)CH}_2\text{-}]_n$ nanocomposites occur. The later mass losses are not found in the 10/c-WO_{3-x}/WO₃×H₂O/[$\text{-Si(O)CH}_2\text{-}]_n$ with the lowest nanowhiskers content. The significant mass losses at above 1000 °C in 20/c-WO_{3-x}/WO₃×H₂O/[$\text{-Si(O)CH}_2\text{-}]_n$ and 30/c-WO_{3-x}/WO₃×H₂O/[$\text{-Si(O)CH}_2\text{-}]_n$ nanocomposites are because of the formation of CO molecules as confirmed by STA-IR (Figure 5b in the main manuscript).

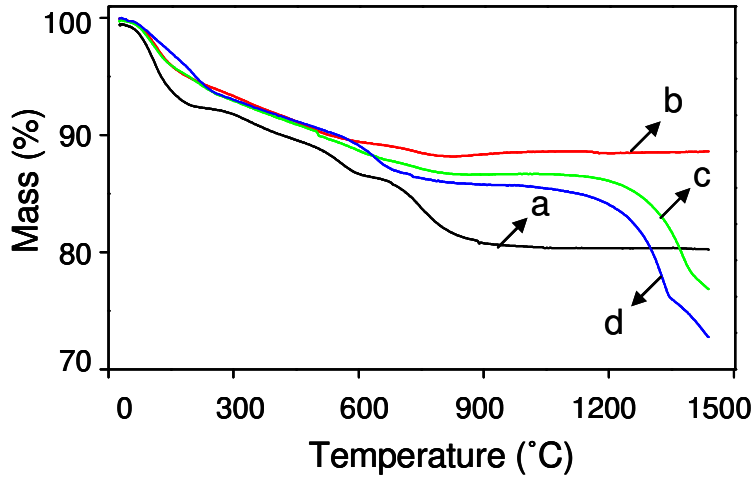


Figure S5. Thermal gravimetric analysis of the (a) $[-\text{Si(O)CH}_2]_n$, (b) 10/c-WO_{3-x}/WO₃ \times H₂O/[$-\text{Si(O)CH}_2]$ _n, (c) 20/c-WO_{3-x}/WO₃ \times H₂O/[$-\text{Si(O)CH}_2]$ _n, (d) 30/c-WO_{3-x}/WO₃ \times H₂O/[$-\text{Si(O)CH}_2]$ _n with 0, 10, 20 and 30 wt % of c-WO_{3-x}/WO₃ \times H₂O nanowhiskers, respectively.

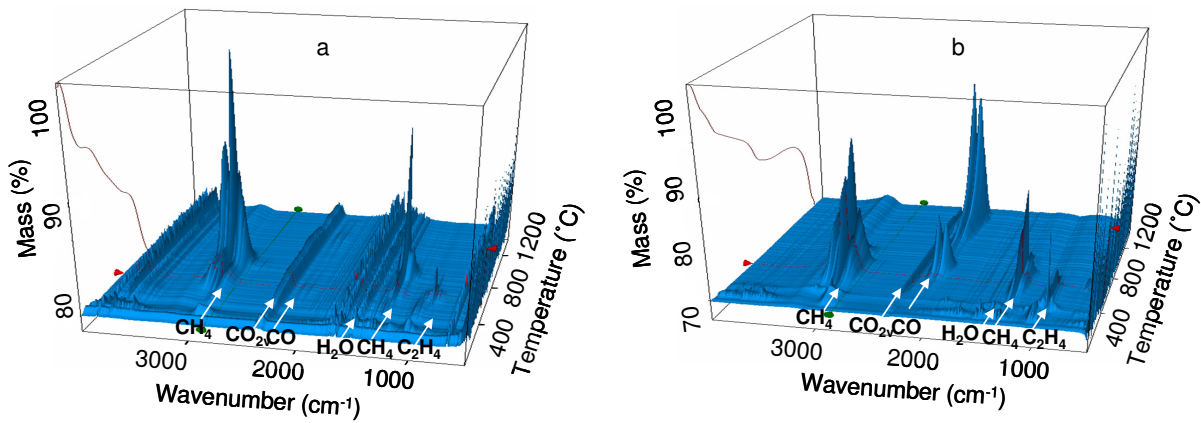


Figure S6. Simultaneous thermal gravimetry (dashed lines left)- infra red analysis (blue areas) for the $[-\text{Si(O)CH}_2]_n$ hybrid polymer (a) and 30/c-WO_{3-x}/WO₃ \times H₂O/[$-\text{Si(O)CH}_2]$ _n nanocomposite (b). The evolution gases H₂O (1511-1504 cm⁻¹) (a), CO (2187-2172 cm⁻¹ and 2116-2098 cm⁻¹) (b), C₂H₄ (953-946 cm⁻¹) (c) and CH₄ (3019-3009 cm⁻¹ and 1306-1301 cm⁻¹) are indicated.

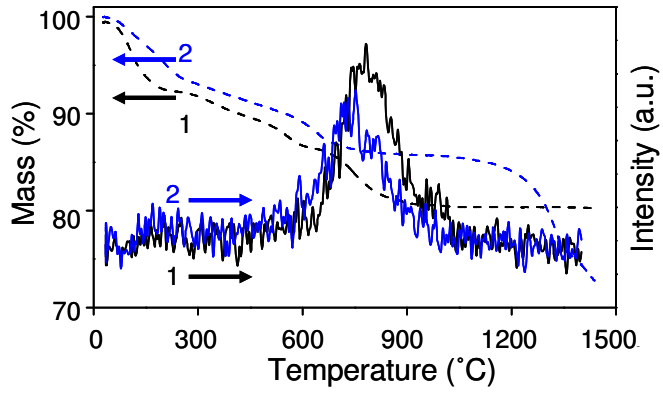


Figure S7. Simultaneous thermal analysis (dashed lines, primary Y axis) coupled with mass spectrometry (solid lines, H₂ (m/z: 2), secondary Y axis) during thermolysis of [-Si(O)CH₂-]_n hybrid polymer (1, black) and 30/c-WO_{3-x}/WO₃×H₂O/[-Si(O)CH₂-]_n nanocomposite (2, blue).

FTIR spectrum of WN/SiOC(N)

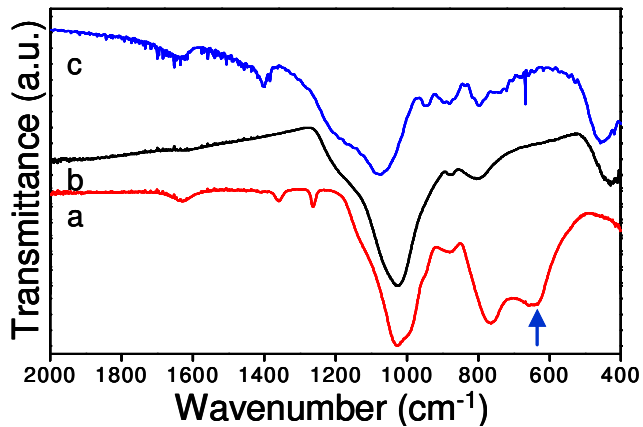


Figure S8. FTIR spectra 30/c-WO_{3-x}/WO₃×H₂O/[-Si(O)CH₂-]_n (a) and after its thermolysis under Ar and NH₃ atmospheres at 800 °C (b) and (c), respectively. The stretching O–W–O vibration at 641 cm⁻¹ is indicated with a blue arrow.

Nitrogen physisorption isotherms and analysis of porosity

The nitrogen physisorption isotherms of the [-Si(O)CH₂-]_n hybrid polymer and the c-WO₃_x/WO₃×H₂O/[-Si(O)CH₂-]_n nanocomposites, as well as their thermolysis products at 700-1300 °C are shown in Figure S9(I-IV).

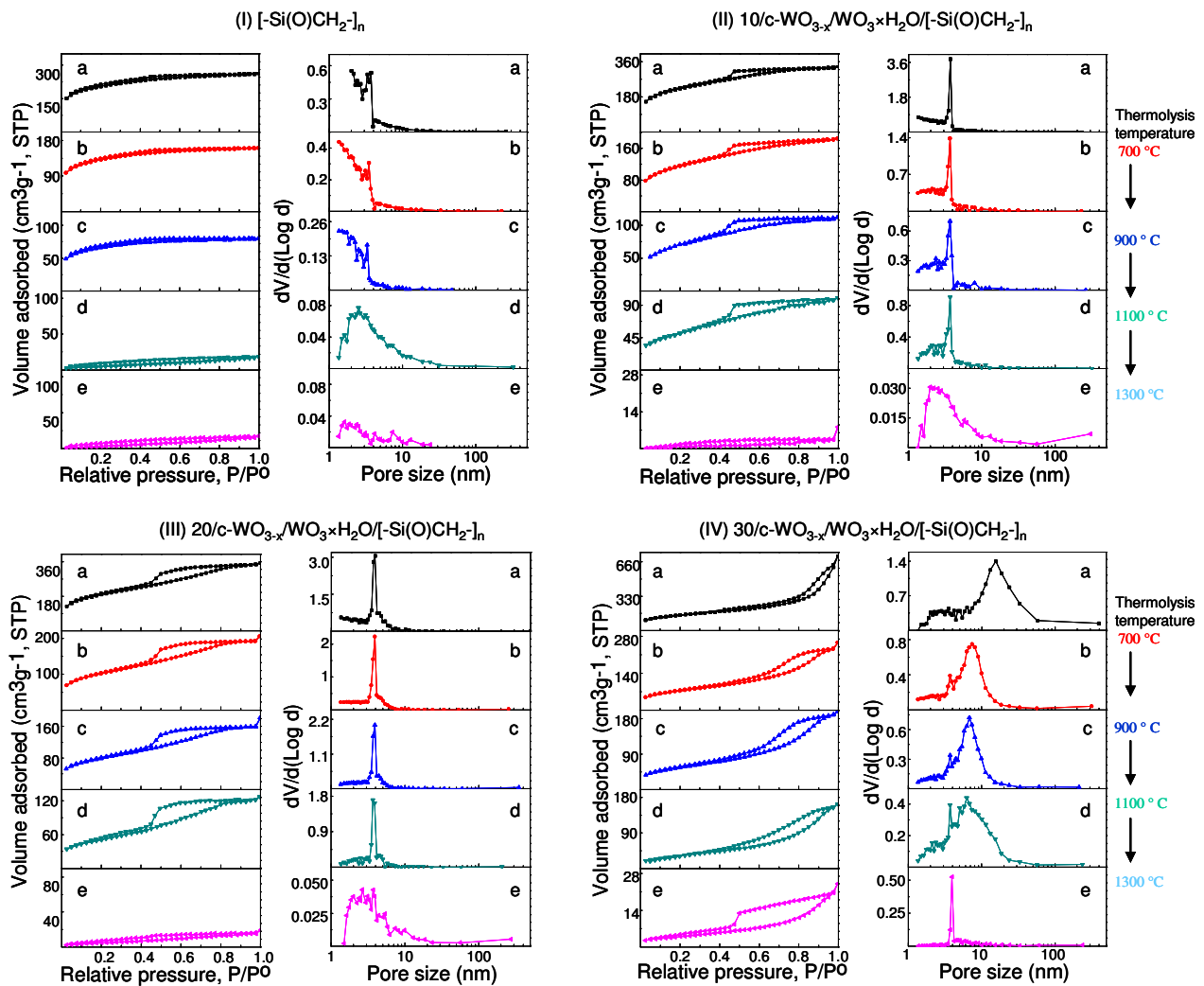


Figure S9. Nitrogen physisorption isotherms (left) and corresponding pore size distributions (right) of $[-\text{Si}(\text{O})\text{CH}_2]_n$ (I), $10/\text{c}-\text{WO}_{3-\text{x}}/\text{WO}_3\times\text{H}_2\text{O}/[-\text{Si}(\text{O})\text{CH}_2]_n$ (II), $20/\text{c}-\text{WO}_{3-\text{x}}/\text{WO}_3\times\text{H}_2\text{O}/[-\text{Si}(\text{O})\text{CH}_2]_n$ (III), and $30/\text{c}-\text{WO}_{3-\text{x}}/\text{WO}_3\times\text{H}_2\text{O}/[-\text{Si}(\text{O})\text{CH}_2]_n$ (IV) with 0, 10, 20 and 30 wt % of c- $\text{WO}_{3-\text{x}}/\text{WO}_3\times\text{H}_2\text{O}$ nanowhiskers, respectively, after synthesis (a), and thermolysis at 700 °C (b), 900 °C (c), 1100 °C (d), and 1300 °C (e).

The $[-\text{Si}(\text{O})\text{CH}_2]_n$ hybrid polymer and its thermolysis products till 900 °C reveal type I nitrogen physisorption isotherm, which is typical for microporous materials (Figure S9(I a-c)), however, the specimens produced at 1100 and 1300 °C are non-porous (Figure S9(I d-e)).

On the other hand, the $10/\text{c}-\text{WO}_{3-\text{x}}/\text{WO}_3\times\text{H}_2\text{O}/[-\text{Si}(\text{O})\text{CH}_2]_n$ and $20/\text{c}-\text{WO}_{3-\text{x}}/\text{WO}_3\times\text{H}_2\text{O}/[-\text{Si}(\text{O})\text{CH}_2]_n$ nanocomposites, as well as their thermolysis products till 1100 °C show type IV

nitrogen physisorption isotherms with type H2 loops, which are common for mesoporous materials with ink-bottle-shaped pores, Figure S9(II a-d and III a-d), respectively.

The 30/c-WO_{3-x}/WO₃×H₂O/[Si(O)CH₂-]_n nanocomposite with the highest content of c-WO_{3-x}/WO₃×H₂O nanowhiskers and its thermolysis products till 1100 °C exhibit type V nitrogen physisorption isotherms characteristic for mesoporous materials with type H3 loops, resulting from wedge-shaped or slit-shaped pores, Figure S9(III a-d). However, the mesoporous structure at 1300 °C shows a type IV nitrogen physisorption isotherm with type H2 loops (Figure S9(IV e)).